JPhys Materials

PAPER • OPEN ACCESS

# Intrinsic defects in and electronic properties of $\theta$-$Al_{13}Fe_4$: an *ab initio* DFT study

To cite this article: C M Fang *et al* 2019 *J. Phys. Mater.* **2** 015004

JPhys Materials

OPEN ACCESS

RECEIVED
10 September 2018

REVISED
13 November 2018

ACCEPTED FOR PUBLICATION
4 December 2018

PUBLISHED
11 January 2019



PAPER

# Intrinsic defects in and electronic properties of $\theta$-$Al_{13}Fe_4$: an *ab initio* DFT study

**C M Fang, A Dinsdale, Z P Que and Z Fan**

BCAST, Brunel University London, Uxbridge, UB8 3PH, United Kingdom

**E-mail:** Changming.Fang@brunel.ac.uk

**Keywords:** $\theta$-$Al_{13}Fe_4$, intrinsic defects, magnetic properties, density-functional theory calculations, phase stability

## Abstract

$\theta$-$Al_{13}Fe_4$ exhibits a rich variety of crystal physics. It contains twenty crystallographically different atomic species with a diversity of chemical coordination. An understanding of its structural and physical properties is a prerequisite for controlling its formation and its use. Here we investigate systematically the intrinsic defects in $\theta$-$Al_{13}Fe_4$ using a first-principles density-functional theory method. The calculations reveal that among the various intrinsic defects it is energetically favourable for Fe substitution of Al but on just three of the fifteen Al sites. This results in a new structural model, $Al_{68}Fe_{24}(Al,\ Fe)_4{}^{IX}(Al,\ Fe)_2{}^{VII}(Al,\ Fe)_4{}^{V}$ (the Roman numerals represent the Al sites) which updates the thermodynamic model, currently in use, which is associated with the formation of vacancies on some of the Al sites. The calculations demonstrate that the addition of Fe induces magnetism which gives rise to clustering. The calculations provide the dependence of the lattice parameters on Fe concentration and explain the experimental data in the literature. The information obtained here provides insight into the formation and properties of $\theta$-$Al_{13}Fe_4$ and its role in the solidification of Al alloys, in determination of the microstructure and related mechanical properties of the products, and in catalysis for organic reactions.

## 1. Introduction

Our interest in $\theta$-$Al_{13}Fe_4$ arises from both scientific curiosity and practical interest. Firstly, $\theta$-$Al_{13}Fe_4$ has a rich variety of crystallography. It exhibits a monoclinic lattice which contains 15 crystallographically different Al types and 5 Fe species, in total 102 atoms (78 Al and 24 Fe atoms) for the chemically stoichiometric composition [1, 2]. The Fe atoms have coordination numbers ranging from 9 to 11 with Fe-Al bonds shorter than 3.0 Å. In contrast the coordination numbers of the Al atoms vary from 10 to 12, except for Al2 which has 6 bonds shorter than 3.0 Å and another 6 slightly longer bonds with lengths between 3.0 to 3.2 Å. This structure was regarded as an approximant of the corresponding quasicrystal [3, 4]. Secondly, the rich diversity of the metallic species indicates the possibility of dissolving other metallic atoms to form multicomponent crystals. Information about $\theta$-$Al_{13}Fe_4$ is very helpful to understand the formation, stability and structural properties of related intermetallic compounds and their role in heterogeneous nucleation processes [5, 6]. Thirdly, iron is regarded as a harmful impurity in many Al alloys [5, 7]. Fe has a very low equilibrium solubility in crystalline Al (<0.05%) and it forms as intermetallic compounds during solidification of Al alloys [5, 6]. Fe containing intermetallic compounds, including $\theta$-$Al_{13}Fe_4$, have a detrimental impact on the properties of both primary and recycled Al alloys [5, 6]. Information about $\theta$-$Al_{13}Fe_4$ and related intermetallic compounds is very helpful to control the harmful Fe impurities in casting Al alloys which is becoming ever more important as the demand for recycling of Al scrap materials increases. Furthermore, it has been recently demonstrated that $\theta$-$Al_{13}Fe_4$ has potential applications as a low-cost and environmentally benign catalyst for organic reactions [8].

The crystal structure of stoichiometric $\theta$-$Al_{13}Fe_4$ is now well defined due to experimental and theoretical studies [1, 2, 9–13]. Early x-ray diffraction patterns suggested that this compound has an orthorhombic lattice [12]. Careful structural analysis showed twinning of crystals, which resulted in an orthorhombic pseudo-symmetry [9]. Black determined the crystallographic structure of $\theta$-$Al_{13}Fe_4$ to be monoclinic with a space group

C2/m (nr. 12) and $a = 15.489$ Å, $b = 8.0831$ Å, $c = 12.476$ Å, $\beta = 107.72°$ [1]. Structural refinements from single crystal samples provided the coordinates of atoms in the unit cell [2, 13, 14].

There have been various discussions about the chemical composition and physical properties of $\theta$-$Al_{13}Fe_4$ [2, 13, 14]. Grin *et al* reported their structural determination of $\theta$-$Al_{13}Fe_4$ [2]. If all lattice sites are occupied this gives the composition $Al_{78}Fe_{24}$ i.e. $Al_{13}Fe_4$ and this represents the most Al rich composition of the phase according to the phase diagram. Grin *et al* [2] also indicated that one site, which they label as Al(2), has partial occupation of 92% or the presence of structural vacancies, although it is not clear how this is possible if the stoichiometry is exactly $Al_{13}Fe_4$. Their structure can be described as $Al_{74}Fe_{24}(Al_{1-x}Va_x)_4{}^{II}$, here Va represents vacancy, $x = 0.08$ and the Roman numeral II indicates the Al2 site [2]. This structural model has been widely used in an analysis of the thermal stability and phase relations of the Al-rich part of the Al-Fe system [15–19]. On the other hand Popčević *et al* performed single crystal structure determinations and observed no vacancy defects in the crystal [13]. Experiments also suggested that samples of $\theta$-$Al_{13}Fe_4$ were magnetic [13] although the results were found to depend on composition and thermal treatments, impurities, etc. In order to address this issue, parameter-free first-principles methods may be used. Early first-principles studies focused on the quasicrystalline nature and electronic properties of $\theta$-$Al_{13}Fe_4$ [4]. Attention was also paid to the stability of the phase at the stoichiometric composition [17, 20], the surface structure and the electronic and catalytic properties of this crystal [21, 22]. Moreover, the first-principles calculations revealed the non-spin-polarization solution of $\theta$-$Al_{13}Fe_4$ [17, 20–23], which differs from the results of experiments [13].

Up to now, there appears to have been no detailed crystal structure determinations on compositions away from the stoichiometry of $\theta$-$Al_{13}Fe_4$ to indicate where defects arise (either from vacancy formation or from substitution). Griger *et al* [24] have prepared samples at different conditions and observed the variation of lattice parameters across the composition range. They reported that the lattice parameters vary linearly, and the unit cell volume decreases as the iron content increases. They explained this in terms of the substitution of Al atoms by Fe leading to a shortening of bond lengths, noting that the Goldschmidt radius of Fe is significantly lower than that of Al. In the present study we investigate, in a systematic way, intrinsic defects, including interstitials, vacancies and substitutions in and related electronic properties of $\theta$-$Al_{13}Fe_4$ using a parameter-free first-principles density-functional theory (DFT) method. Our study demonstrates that there should be hardly any vacancy defects in $\theta$-$Al_{13}Fe_4$ and that the dominating defect accounting for the range of homogeneity should be the replacement of Al by Fe in three of the fifteen Al sites. Based on these calculations, a new structural model has been proposed, which updates the model used hitherto for the thermodynamic properties. Magnetism and its origin in the nonstoichiometric $\theta$-$Al_{13}Fe_4$ configurations are also addressed.

## 2. Computational details

### 2.1. Formation energy and defect energy

To have a measure of the relative stability of the $Al_{13}Fe_4$ phase, the formation energy ($\Delta E_f$) with respect to the elemental solids ($\alpha$-Al, $\alpha$-Fe) is defined [25, 26] as:

$$\Delta E_f = [E(Al_{13}Fe_4) - \{13E(Al) + 4E(Fe)\}]/17. \quad (1)$$

In this paper the unit of formation energy, $\Delta E_f$, will be given in eV/atom. Here $E(Al_{13}Fe_4)$ is the calculated total valence electron energy for the compound, $E$(Al) and $E$(Fe) are the equivalent values for pure Al and Fe, respectively.

For the intermetallic structures caused by substitution, the formation energy of the defects is defined in terms of the unit cell where the formula is now $Al_{78}Fe_{24}$:

$$\Delta E_r = E\{(Al_{1-x}Fe_x)_{78}(Fe_{1-y}Al_y)_{24}\} - \{6E(Al_{13}Fe_4) - (78x - 24y)E(Al) - (24y - 78x)E(Fe)\}. \quad (2)$$

Similarly, for an intermetallic with vacancies, $(Al_{1-x}Va_x)_{78}(Fe_{1-y}Va_y)_{24}$, the formation energy of the defects per unit cell is defined as:

$$\Delta E_{vac} = E\{(Al_{1-x}Va_x)_{78}(Fe_{1-y}Va_y)_{24}\} - \{6E(Al_{13}Fe_4) - 78x\ E(Al) - 24yE(Fe)\}. \quad (3)$$

Naturally, for an intermetallic with interstitial atoms, $(Al_{1+x})_{78}(Fe_{1+y})_{24}$, the formation energy of the interstitial defects ($\Delta E_{int}$) per unit cell is referred as:

$$\Delta E_{int.} = E\{(Al_{1+x})_{78}(Fe_{1+y})_{24}\} - \{6E(Al_{13}Fe_4) + 78x\ E(Al) + 24y\ E(Fe)\}. \quad (4)$$

**Table 1.** Calculated and experimental results (lattice parameters, and formation energy) for $\theta$-$Al_{13}Fe_4$ in comparison with previous available experimental data and theoretical calculations. The formation energy $\Delta E_f$ is defined in equation (1).

| Lattice parameters (Å) | | | | | | |
|---|---|---|---|---|---|---|
| *a* | *b* | *c* | $\beta$(°) | $\Delta E_f$(eV/atom) | Method | References |
| 15.426, | 8.022, | 12.425, | 107.68 | −0.330 | DFT-PBE-GGA | This work |
| Experiment | | | | | | |
| | | | | −0.291 | Direct reaction calorimetry | [35] |
| | | | | −0.272 | Solution calorimetry | [36] |
| | | | | −0.289 | Direct reaction calorimetry | [37] |
| | | | | −0.225 | CALPHAD assessment | [19] |
| | | | | −0.296 | CALPHAD assessment | [16] |
| | | | | −0.310 | CALPHAD | [38] |
| 15.489, | 8.083, | 12.476, | 107.72 | | Powder XRD | [1] |
| 15.49, | 8.08, | 12.48, | 107.40 | | Powder XRD | [4, 36] |
| 15.509, | 8.066, | 12.469, | 107.72 | | Powder XRD | [24, 37] |
| 15.492, | 8.078, | 12.471, | 107.69 | | Powder XRD | [2] |
| 15.488, | 8.0866, | 12.4766, | 107.669 | | Single crystal | [13] |
| 15.503, | 8.063, | 12.464, | 107.71 | | Powder XRD | [39] |
| 15.423, | 8.0535, | 12.408, | 107.86 | | Single crystal | [14] |
| | | | | Theoretical | | |
| 15.069, | 7.864, | 12.083, | — | −0.059 | Atomist. EAM | [34] |
| — | | | | −0.320 | DFT | [40] |
| — | | | | −0.347 | DFT | [17] |
| 15.419, | 8.021, | 12.420, | 107.71 | −0.330 | PBE-GGA | [20] |
| 15.307, | 7.956, | 12.332, | 107.75 | −0.345 | PBEsol | |

The unit for the energy of formation of the defects in equations (2)–(4) is eV per unit cell and the values are relative to the stoichiometric composition, $\alpha$-Al and $\alpha$-Fe.

### 2.2. Computational settings

The plane wave method (using VASP, Vienna *ab initio* Simulation Package) was used for the calculations [27]. The spin-polarized generalized gradient approximation (SP-GGA-PBE) [28] within the projector-augmented wave method [29] was employed for the exchange and correlation energy terms because the spin-polarized generalized gradient approximation describes the 3d transition metals such as Fe better than the (spin-polarized) local density approximation (LDA) [30, 31]. The cut-off energy of the wave functions was set at 550 eV and the cut-off energy of the augmentation functions was 700 eV to describe the rather localized Fe 3d orbitals. The electronic wave functions were sampled on a $4 \times 8 \times 6$ grid with 70–100 $\boldsymbol{k}$-points, in the irreducible Brillouin zone of $\theta$-$Al_{13}Fe_4$ depending on the symmetry using the Monkhorst–Pack method [32]. Note that the Fe 4s, 4p and 3d electrons and Al 3s, 3p electrons exhibit an itinerant character in alloys and in principle belong to the whole crystal. However, we can decompose the plane waves in the atomic sphere and obtain e.g. the Fe 3d components in the spheres for both spin-up (or majority) and spin-down (minority) direction. In this way a local magnetic moment is obtained that is the difference between the spin-up electrons and spin-down electrons in the sphere. To obtain the ground state of the crystals, we performed calculations for different inputs. This avoided the possibility of our results falling into metastable solutions [25, 26, 31]. Both lattice parameters and coordinates of atoms were fully relaxed. Different $\boldsymbol{k}$-meshes and cut-off energies were used for the waves and augmentation waves, respectively. Tests showed good convergence (<1 meV/atom).

## 3. Calculation results

### 3.1. Structure of stoichiometric $\theta$-$Al_{13}Fe_4$

We first discuss the calculations for the elemental solids, $\alpha$-Fe and $\alpha$-Al using the settings discussed earlier. The calculations provide a lattice parameter of 4.039 Å for $\alpha$-Al (face-centred cubic, fcc) and 2.830 Å for $\alpha$-Fe (body-centred cubic, bcc) for 0 K. These calculated lattice parameters agree well with the experimental values, 4.0325 Å for $\alpha$-Al and 2.8607 Å for $\alpha$-Fe also for 0 K (within 1%) [33], respectively. Such good agreement provides confidence in the reliability of the software and the selected settings.

The calculated results (lattice parameters and formation energy) of the stoichiometric $\theta$-$Al_{13}Fe_4$ crystal are summarized and compared with previous experimental and theoretical values published in the scientific literature in table 1. Figure 1 shows the structure of $\theta$-$Al_{13}Fe_4$ schematically.

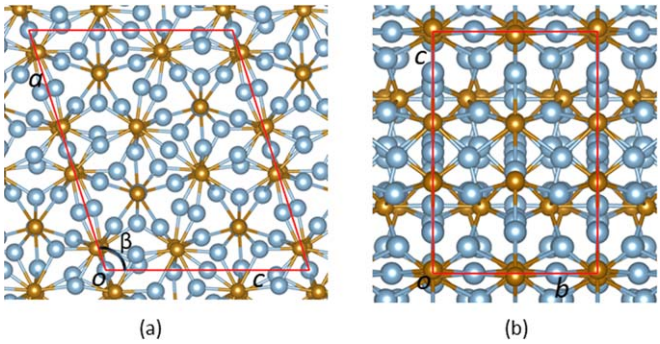


**Figure 1.** Schematic structure along the [010] (a) and the [100] (b) orientation of $\theta$-$Al_{13}Fe_4$. The silvery spheres represent Al and the golden spheres Fe. The red lines represent the axes of the unit cell. O represents the origin, and *a*, *b*, *c* the axis of the unit cell.

As shown in table 1, our calculated lattice parameters are in good agreement (within 1%) with available experimental values and previous first-principles calculations. However, our calculations provided rather larger differences in both lattice parameters and formation energy from data produced by the semi(empirical) embedded atom method [34]. This is due to the difficulties in deriving an EAM potential/model to describe well the intermetallic compounds and the complex interactions between atoms. We have also tested the DFT + $U$ method ($U = 2.91$ eV) for $\theta$-$Al_{13}Fe_4$. The calculations revealed large local magnetic moments (values ranging from 1.3 $\mu_B$/Fe to 1.9 $\mu_B$/Fe), being different from the weak magnetism from the experimental observations [13]. This result is in line with the previous calculations that DFT + $U$ works better than DFT-GGA for ionic compounds, such as oxides but DFT + GGA work works better for covalent intermetallic compounds [31]. As shown in table 1, the experimental measurements of the formation energy for this compound are somewhat scattered. They are thought to be unreliable in that the chemical reactions involved may not have been carried out to completion. Our calculated formation energy is close to some of the recent thermodynamic CALPHAD assessments [16, 38], although it appears to disagree with the most recent value [19]. It is also in good agreement with the previous first-principles calculations within a few percent [17, 20, 40]. The small differences originate from different density functionals, e.g. the LDA [40], or the hybrid method (PBEsol) [20], or from different settings [17]. Our calculations confirmed that the ground state of $\theta$-$Al_{13}Fe_4$ is non-magnetic in agreement with the previous first-principles studies [17, 20, 40].

### 3.2. Intrinsic defects in $\theta$-$Al_{13}Fe_4$

To shed some light on the homogeneity range and structure of $\theta$-$Al_{13}Fe_4$, we investigated different possible intrinsic defects: vacancies in the Fe or the Al sites, substitution of Fe atoms by Al and substitution of Al atoms by Fe. Test calculations of interstitial atoms in the large unoccupied sites, e.g. the Wyckoff 2a or 2b sites in $\theta$-$Al_{13}Fe_4$ [2] revealed that their formation is highly improbable with formation energies over 2 eV/unit cell according to equation (4). Consequently, interstitial defects were not considered further. The calculated formation energies of the defects according to equations (2) and (3) were plotted in figure 2(a).

The calculations provide us with the following information. We use the Grin's notations for the atoms' sites throughout rest of this paper [2]:

(i) The chemically stoichiometric composition of $\theta$-$Al_{13}Fe_4$ has the lowest formation energy at 0 K;

(ii) The formation of vacancies on the Al and/or Fe sites is associated with an increase of energy of over 1 eV/unit cell. Therefore, it is highly improbable that $\theta$-$Al_{13}Fe_4$ will contain appreciable amounts of vacancies on either the Al or Fe sites even at elevated temperatures. This is in contrast to the much-quoted model of Grin *et al* which can be formulated as $Al_{74}Fe_{24}(Al_{1-x}Va_x)_4^{II}$ with $x = 0.08$ with the Roman numeral II designating the Al2 site [2]. However, our results agree with the single crystal structure determinations [13, 14];

(iii) The energy costs are also too high to substitute an Al atom onto an Fe site. Therefore, a model with the formula $Al_{78}(Fe_{1-x}Al_x)_{24}$ which would allow the homogeneity range to extend towards Al rich compositions is unlikely;

(iv) The energy costs to substitute one Fe atom onto an Al site according to the formula $(Al_{1-x}Fe_x)_{78}Fe_{24}$ are reasonably small in the ground state but are limited to three Al sites, Al9 (156 meV/unit cell), Al7 (181 meV/unit cell) and Al5 (188 meV/unit cell); based on the results, we propose a new model with the formula $Al_{68}Fe_{24}(Al,\ Fe)_4{}^{IX}(Al,\ Fe)_2{}^{VII}(Al,\ Fe)_4{}^{V}$, the Roman numerals designating the corresponding Al sites.

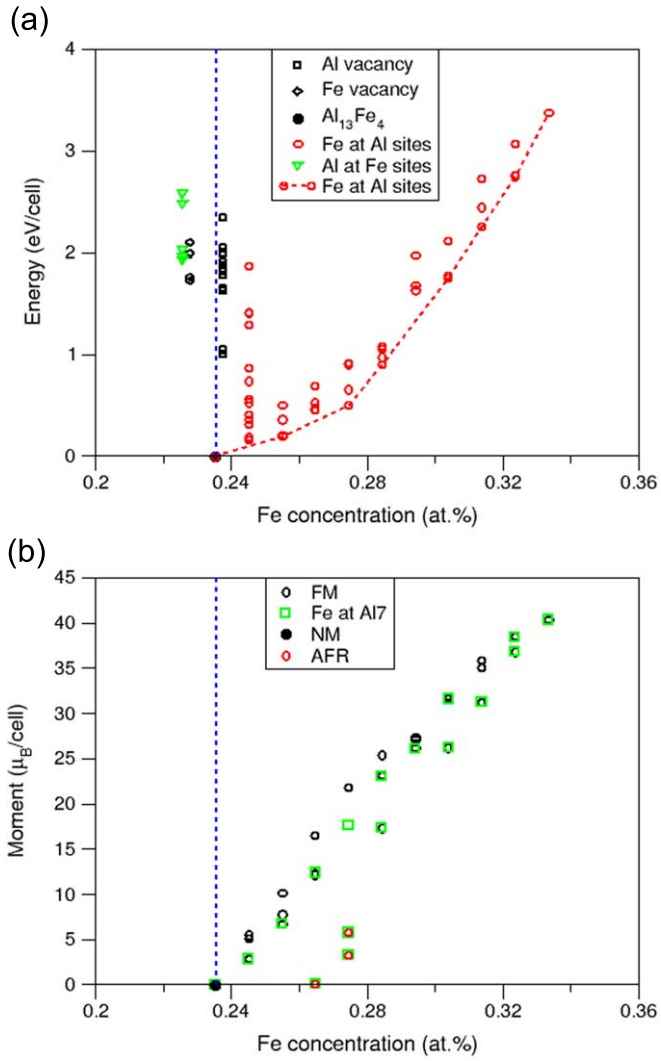


**Figure 2.** Calculated formation energies of defects (eV/cell) at 0 K relative to the stoichiometric composition, fcc Al and bcc Fe according to equations (2) and (3) (a) and the total magnetic moments (b) associated with the introduction of intrinsic defects into the unit cell of $\theta$-$Al_{13}Fe_4$. The vertical dotted blue line in both pictures represents the stoichiometric composition. The dotted red curve in 2(a) connects the most stable configurations. In figure 2(b) the green squares represent the magnetic moments for configurations containing Fe on the Al7 sites. The red spheres represent anti-ferrimagnetic (AFR) ordering with the Al7 sites fully occupied by Fe atoms.

(v) Additions of Fe induce magnetism. The magnetic moments associated with the introduction of defects are shown in figure 2(b). Overall, the magnetic moment of a composition increases with increase of Fe concentration. However, this relationship is complicated by the local magnetic moments and magnetic ordering.

Figure 2(a) also shows that the formation energies for the same chemical composition vary notably. For one Fe addition, the configuration with Fe on the Al9 site (labelled as $Fe^{IX}$) has the lowest formation energy (0.156 eV/unit cell). There are six configurations to add two Fe atoms into the three Al sites, among which two are noticeably more stable, that is two Fe atoms on the Al5 sites (2 $Fe^{V}$) and two Fe atoms on the Al7 sites (2 $Fe^{VII}$). There are 8 independent configurations for three Fe atoms on three Al sites. The most stable are Case I with two Fe atoms on Al7 sites and one Fe atom on an Al5 site ($\Delta E_r = 0.451$ eV/unit cell); and Case II with three Fe atoms on Al9 sites ($3Fe^{IX}$) with $\Delta E_r = 0.472$ eV/unit cell. It is interesting to note that, as shown in figure 2(b), for the systems with three Fe atoms, the calculations predict ferromagnetic behaviour for Case II, in contrast to ferrimagnetic (FRM) behaviour for the most stable configuration, Case I, in which the Al7 sites are fully occupied by Fe atoms. This is in contrast to a configuration with two Fe atoms on Al7 sites and one Fe atom on an Al9 site which exhibits ferromagnetic ordering but with a formation energy of 0.531 eV/unit cell, notably higher than that for Case I. In the configuration Case I, there are two Fe groups, one centred around $Fe^{VII}$ and the other around $Fe^{V}$ (the Roman numerals represent the Al sites). The Fe atoms in the same group display ferromagnetic

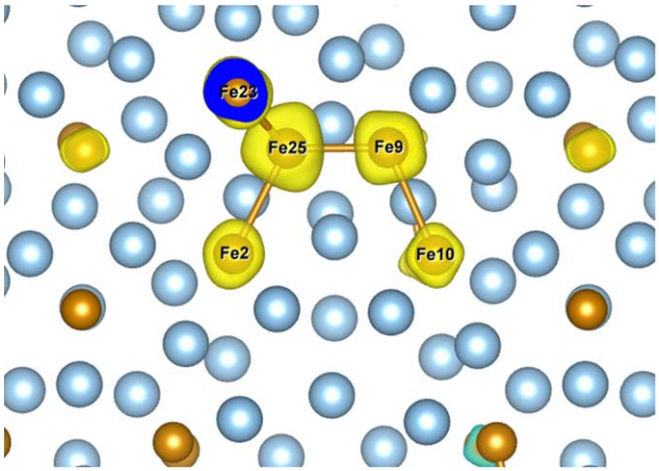


**Figure 3.** Iso-surfaces of spin-density ($\rho(\boldsymbol{r}) = 0.007$ e Å$^{-3}$) for an iron cluster centred at Fe25 of the Al9 site along the (010) orientation of the lattice. The iso-surfaces are indicated by yellow spheres, the blues regions signify higher density. The gold spheres represent Fe and the silver spheres, Al atoms.

**Table 2.** Calculated chemical bonds and local magnetic moments of the clustered Fe atoms which are centred around an Fe atom substituting in Al9, Al7 and Al5 sites. The species with the iron numbered as Fe_22, Fe_23, etc are labelled in parenthesis and shown in figure 4. The radius of the Wigner spheres of iron is 1.01 Å.

| Fe on Al9(site) | $d_{Fe*\text{-}Fe}$ (Å) | M ($\mu_B$) | Fe on Al7(site) | $d_{Fe^*\text{-}Fe}$ (Å) | M ($\mu_B$) | Fe on Al5(site) | $d_{Fe^*\text{-}Fe}$ (Å) | $M$ ($\mu_B$) |
|---|---|---|---|---|---|---|---|---|
| Fe* (Al9) | — | 2.21 | Fe* (Al7) | — | 1.82 | Fe* (Al5) | — | 2.26 |
| Fe_9 (Fe3) | 2.48 | 1.23 | Fe_5(Fe2) | 2.56 | 0.67 | Fe9 (Fe3) | 2.52 | 0.78 |
| Fe_22(Fe5) | 2.47 | 0.76 | Fe_6(Fe2) | 2.56 | 0.67 | Fe13(Fe4) | 2.47 | 0.84 |
| Fe_23(Fe) | 2.47 | 0.76 | | | | | | |
| Fe_2 (Fe1) | 2.90 | 0.49 | | | | | | |
| $M_{total}$($\mu_B$/cell) | — | 5.58 | | | 2.86 | | | 5.10 |

ordering but they are anti-parallel to the members of the other group. As shown in figure 2(b), such magnetic behaviour also occurs for the configuration with (a) $2Fe^{VII}$ and $2Fe^{V}$, which is the most stable, and (b) $2Fe^{VII}$ and $1Fe^{V}$ and $1Fe^{IX}$. The calculations also showed that the configuration with $2Fe^{VII}$ and $2Fe^{IX}$ is ferromagnetic and has a higher formation energy. Configurations with further Fe additions are calculated to be ferromagnetic (figure 2(b)). The most stable configuration for five Fe additions is the one displaying ferromagnetic behaviour with $2Fe^{VII}$ and $3Fe^{V}$ ($\Delta E_r = 0.901$ eV/unit cell). Further addition of Fe causes the formation energies to be higher than one eV/unit cell relative to that of the stoichiometric composition and, therefore, unlikely to form even at elevated temperatures in Al alloys.

### 3.3. Magnetic clustering

Next, we discuss the distribution of local magnetism in the cell of the $\theta$-$Al_{13}Fe_4$ crystals using the dilute replacement of Fe in the three Al sites as examples. The results are shown in table 2. Figure 3 displays a typical distribution of the spin-density for the most stable case, (one Fe at one Al9 site). Table 2 shows that the short Fe-Fe distances and related magnetic moments of the doped Fe are close to those of bulk $\alpha$-Fe [41, 42]. The induced local magnetic moments at other Fe spheres range from between 0.6 and 1.2 $\mu_B$/Fe.

To obtain some further insight into the origin of magnetism introduced by the addition of Fe, we performed electronic structure calculations for spin-polarized and non-spin-polarized configurations of the system with the substitution of one Fe atom onto the Al sites. The calculations showed high stability of magnetic configurations for the substitution of Fe atoms with significant energy differences between the spin-polarized and the non-spin-polarized configurations. For example, the energy difference between the spin-polarization configuration and the non-spin-polarization configuration is 0.386 eV/unit cell for the substitution of one Fe onto the Al9 site. The calculated partial density of the 3d states of the related iron atoms is shown in figure 4.

Figure 4(b) shows that for the non-spin-polarized solution the density of the 3d states at the Fermi level is high for the related Fe atoms: $\rho(E_{Fermi}) = 3.7$ states/eV for Fe_25, 2.8 states/eV for Fe9, 1.5 states/eV for Fe_22 and Fe_23, and 1.6 states/eV for Fe2. The $\rho(E_{Fermi})$ value of Fe_25 3d states is close to that of non-spin-polarized solution of $\alpha$-Fe [41–43]. It is expected that such high density of the itinerant Fe 3d states

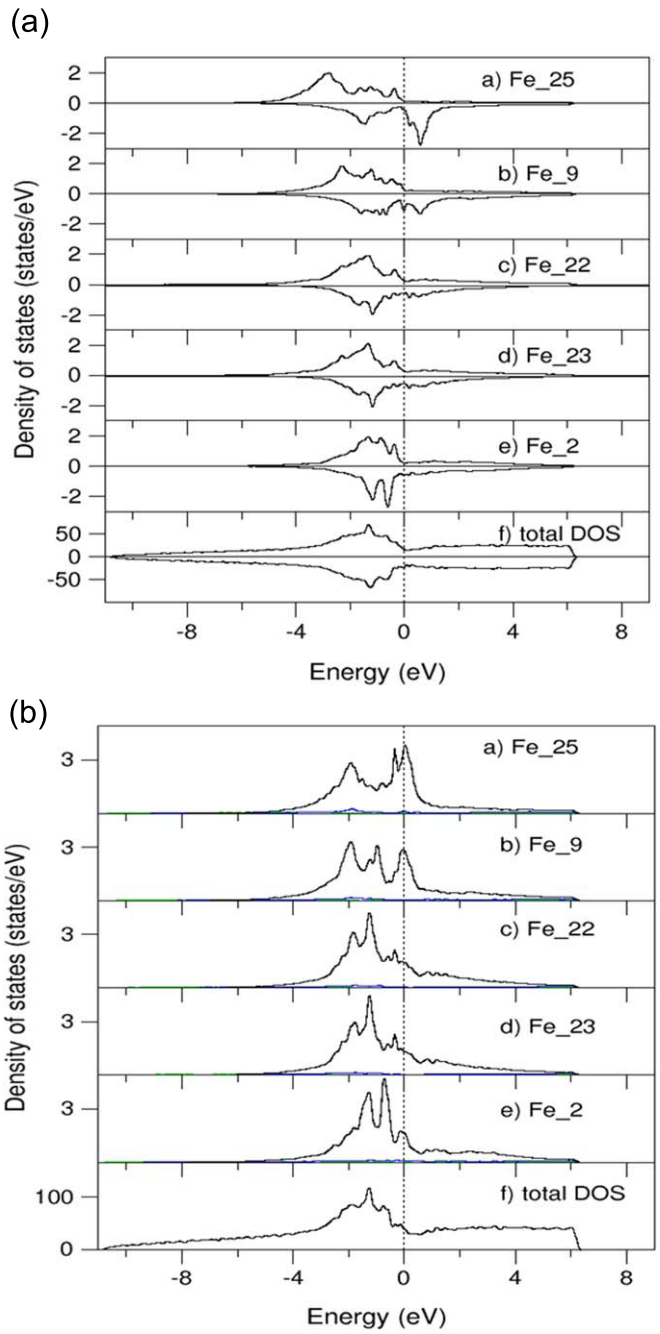


**Figure 4.** The partial densities of the 3d states of the magnetic Fe atoms/ion (a) and non-spin-polarized solution (b) in the one Fe addition in the Al9 sites in $\theta$-$Al_{13}Fe_4$. The labels of Fe atoms are the same as in table 2 and figure 3.

at the Fermi level will cause spin-polarization splitting which occurs in many cases according to the Stoner criteria [44, 45].

Figure 4(a) shows that the 3d states of the added Fe atom are almost fully spin-polarized: the Fe 3d states of the spin-up states are almost fully occupied while the Fermi level falls in the pseudo-gap of the Fe 3d states for the spin-down (minority) electrons. This behaviour is very similar to that of pure $\alpha$-Fe [41–43]. The induced local moments are noticeably smaller, ranging from 0.49 to 1.23 ($\mu_B$/unit cell) as shown in table 2. The Fe atoms which are connected to other Fe atoms that have been magnetically induced by the added Fe, also become magnetic with a smaller local moment, typically smaller than 0.35 ($\mu_B$/unit cell). Figures 3 and 4 show, as an example, that the Fe10, which is directly connected to Fe9, is magnetic and has a local moment of 0.33 ($\mu_B$/unit cell). Therefore, the total magnetic moment in the unit cell is different for the Fe addition on different Al sites: 5.58 $\mu_B$/cell for Fe on Al9, 2.86 ($\mu_B$/unit cell) for one Fe on Al7 and 5.10 ($\mu_B$/unit cell) for one Fe on Al5 site (table 2).

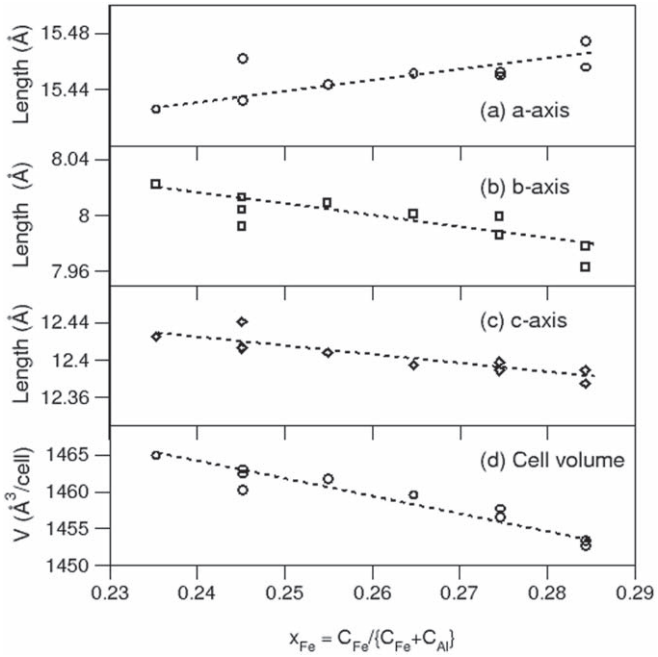


**Figure 5.** Variation of calculated lattice parameters and cell volume with Fe concentration in $\theta$-$Al_{13}Fe_4$ samples.

### 3.4. Dependence of lattice parameters on Fe concentration

Griger *et al* reported their measurements for $\theta$-$Al_{13}Fe_4$ of the dependence of the lattice parameters on the mole fraction [24]. These relations were considered to be helpful in order to measure the Fe concentrations of samples prepared under different conditions. Therefore, we also analysed the dependence of lattice parameters and the cell volume on the Fe concentration up to about 28.5 at% Fe. The results are plotted in figure 5.

The general trend is that the length of the *a*-axis increases, while the lengths of *b*- and *c*-axis decrease with increase of Fe concentration (figure 5) for Fe concentrations lower than 0.29. This is in line with the experimental measurements of Griger *et al* [24]. However, this trend is complicated by the anomalous behaviour of configurations with Fe occupation on the Al7 sites ($Fe^{VII}$). In figure 5, the larger values of the length of the *a*-axis correspond to configurations of Fe on the Al7 sites. This is also true for other configurations containing $Fe^{VII}$. Furthermore, the calculations also showed that the length of the *a*-axis decreases with Fe concentration ($X_{Fe}$) when $X_{Fe}$ is higher than 30 at%. Therefore, caution should be taken when one tries to use the dependence of lattice parameters on the Fe mole fraction as a measure of the Fe concentration of the samples. Meanwhile the *b*-axis of the configurations of $Fe^{VII}$ is shorter than that of the others. As a result, the overall cell volume decreases with an increase of Fe concentration.

## 4. Discussion

### 4.1. Fe fraction and magnetism in $\vartheta$-$Al_{13}Fe_4$ at elevated temperature

Our calculations showed that the stoichiometric composition of $\theta$-$Al_{13}Fe_4$ has the lowest formation energy relative to the pure elements and is non-spin-polarized or non-magnetic. However, the calculations also showed that the replacement of Al atoms by Fe on three Al sites (Al5, Al7 and Al9) has only a moderate energy penalty. The defect energy cost for this type of replacement is about 0.156 eV per unit-cell to 0.188 eV per unit-cell. The defect energy increases with Fe concentration. Therefore, at low temperatures, $\theta$-$Al_{13}Fe_4$ should be approximately stoichiometric at thermodynamic equilibrium. However, the addition of Fe atoms on the Al sites induces (i) an increase in the number of configurations with different Fe/Al occupation or extra freedom of atomic occupation, and (ii) magnetism of the system. According to thermodynamics, at elevated temperature, the Gibbs energy of a system can be represented as $G = H - TS$ at the pressure $p = 0$ Pa. The extra freedom of occupation produces a configurational entropy, $S = k_B \ln w$, here $k_B$ is the Boltzmann constant and $w$ is the number of independent configurations. This contribution can be calculated, e.g. for one Fe on the Al9 site ($w = 4$), $TS = 0.120$ eV for $T = 1000$ K or 0.168 eV for $T = 1400$ K. The latter value is larger than the cost of the defect energy. The calculations showed that the $\theta$-$Al_{13}Fe_4$ phase with the addition of Fe develops ordered magnetic structures (ferromagnetic (FM) or ferrimagnetic (FRM)). The Fe atoms substituted into the Al sites

have neighbours on the Fe sites with the Fe–Fe interatomic distances range from 2.45 to 3.12 Å. The shorter interatomic distances associated with Fe substitution on the Al 4i sites (Al5 and Al9) are approximately the same as that in $\alpha$-Fe. The 3d–3d bond between Fe atoms causes high density of the itinerant Fe 3d states and therefore, spin-polarization splitting occurs. In principle the Curie–Weiss magnetic ordering contribution to the Gibbs energy of the system can be calculated since we have obtained the local magnetic ordering. However, the calculations showed Fe magnetic clustering and a variation of local magnetic moments within the Fe clusters. The variations of the Fe–Fe interatomic distances and local magnetic moments indicate a variation of Curie–Weiss transition temperatures in the Fe clusters. This is further complicated by the formation of different Fe clusters in the alloys formed at elevated temperatures (1000 to 1500 K). Therefore, the currently used models in the scientific literature [24, 41–43] cannot be applied directly to the magnetic transitions associated with Fe clustering in the Al-Fe intermetallic compounds. However, we may estimate the contributions of the Curie–Weiss magnetic ordering to the thermal stability. BCC Fe has a local moment of 2.22 $\mu_B$/Fe and a Curie temperature of 1043 K. The contribution to the thermal enthalpy due to the Curie–Weiss magnetic ordering is $-9180.56$ J mol$^{-1}$ or $-95.1$ meV/Fe. Our calculations showed that for one Fe on the Al9 site, there are 5 Fe atoms which are associated with magnetism with a total moment of about 5.6 $\mu_B$/unit cell or about 1.1 $\mu_B$/Fe. If we assume a linear relation between the magnetic moment and the enthalpy associated with magnetic ordering, then we obtain that the contribution of the magnetic ordering at elevated temperatures ($\Delta H_{mag}$) is about $-0.234$ eV/unit cell. If we apply the same approach for one Fe on an Al7 site, we obtain $\Delta H_{mag} = -0.123$ eV/unit cell. Therefore, at high temperature, the contribution of the extra freedoms of the irons spins (Curie–Weiss magnetic transition) further stabilizes the defective structures.

Samples of the $\theta$- $Al_{13}Fe_4$ phase are generally prepared at high temperature as primary or secondary intermetallic compounds in Al alloys. At such high temperatures, the samples in thermal equilibrium should contain higher Fe concentrations in the three Al sites. The obtained composition and structure may be retained as the alloys are cooled to low temperatures. The composition and the specific location of the defects will depend strongly on the preparation conditions and thermal history. This could explain the scattering of experimental observations including the magnetic properties in the literature.

### 4.2. Thermodynamic model for $\vartheta$-$Al_{13}Fe_4$

This work provides a new understanding of the nature of intrinsic defects in $\theta$-$Al_{13}Fe_4$ which should be reflected in a new way to represent its thermodynamic properties. The model used previously in thermodynamic assessments is generally represented as $(Al)_{.6275}(Fe)_{.235}(Al, Va)_{.1375}$ [16–18] which, in terms of the unit cell, can be displayed as $(Al)_{64.005}(Fe)_{23.97}(Al, Va)_{14.025}$. Clearly this provides the possibility for a much wider range of homogeneity than implied from the results of Grin *et al* [2], $(Al)_{74}(Fe)_{24}(Al, Va)_4$ which has been used as justification for the inclusion of vacancies. This flexibility, which allows for this wider range of homogeneity, is not necessary for the Al-Fe system itself but would be necessary to model the extent of the homogeneity range of the phase in e.g. the Al-Fe-Mn system [46]. In this paper we have shown that formation of vacancies is very unfavourable energetically and that substitution of Fe onto three of the Al sites is much more plausible leading to the thermodynamic model $Al_{68}Fe_{24}(Al, Fe)_4(Al, Fe)_2(Al, Fe)_4$. Even this description is not sufficient to represent the complexity of the phase. As shown earlier, substitution of Fe onto Al sites causes the phase to become magnetic. Simultaneous substitution of two Fe atoms on different sublattices leads to magnetic clustering and further lowering of the energy. Furthermore, at higher temperatures it might be expected that the contribution to the Gibbs energy from configurational entropy will lead to mixing on all of these three Al sites. It is therefore suggested an appropriate thermodynamic model to use for thermodynamic analyses of the $\theta$-$Al_{13}Fe_4$ in ternary systems is $Al_{68}Fe_{24}(Al, Fe)_{10}$.

## 5. Conclusions

We performed first-principles calculations on the structural and electronic properties of $\theta$-$Al_{13}Fe_4$. Our calculations showed that at low temperature the chemically stoichiometric composition of $\theta$-$Al_{13}Fe_4$ has the lowest energy of formation. It is also non-magnetic. These results agree well with the previous papers in the scientific literature. The calculations also reproduced the experimental lattice parameters in the scientific literature to within 1%. Vacancies are unlikely to be present on either Al or Fe sites. The energy associated with substitution of Fe on Al sites suggests that it is possible but limited to three sites only, Al9, Al7 and Al5. Therefore, the structures of the $\theta$-$Al_{13}Fe_4$ can be described as $Al_{68}Fe_{24}(Al, Fe)_4{}^{IX}(Al, Fe)_2{}^{VII}(Al, Fe)_4{}^{V}$, which is in contrast to the accepted description $Al_{74}Fe_{24}(Al, Va)_4{}^{II}$, following the work of Grin *et al* [2], where here the Roman numerals represent the specific Al sites, and Va indicates a vacancy. Substitution of Fe also induces magnetism, which agrees with the experimental observations. This magnetic contribution together with a configurational contribution stabilizes the defect containing $\theta$-phase at elevated temperatures. The calculations also showed

some general trends in the dependence of the lattice parameters and cell volume on Fe fraction. The magnetism of the samples with excess Fe may help to remove Fe in recycling of scrap Al alloys, and to get some insight into the catalysis of this compound for organic reactions. The obtained information is further helpful to formulate a new model to represent the thermodynamic properties of the phase for use in the critical assessment of thermodynamic and phase diagram data for Al-Fe-X ternary and multicomponent systems and the calculation of phase equilibria.

## Acknowledgments

EPSRC is gratefully acknowledged for supporting the EPSRC Centre under grant EP/H026177/1.

## ORCID iDs

C M Fang https://orcid.org/0000-0003-0915-7453

## References

[1] Black P J 1955 *Acta Crystallogr.* **8** 175
[2] Grin J, Burkhardt U, Ellner M and Peters K 1994 *Z. Kistallogr.* **209** 479
[3] Gille P and Bauer B 2008 *Cryst. Res. Technol.* **43** 1161
[4] Cabera-Trujillo J M, Morán-López J L and Kumar V 1992 *J. Phys.: Condens. Matter* **5** A399
[5] Zhang L F, Guo J W, Nana L, Damoah W and Robertson D G 2012 *Miner. Process. Extractive Metall. Rev.* **33** 99
[6] Que Z P, Zhou Y P, Wang Y and Fan Z 2017 *Proc. 6th decennial international conference on solidification processing* p 158
[7] Bäckerud L, Król E and Tamminen J 1986 *Solidification, Characteristics of Aluminium Alloys* (Oslo: Skan Aluminium)
[8] Armbrüster M *et al* 2012 *Nat. Mater.* **1** 690
[9] Black P J 1955 *Acta Crystallogr.* **8** 43
[10] Hudd R C and Taylor W H 1962 *Acta Crystallogr.* **15** 441
[11] Yanson T I, Manyako N B, Bodak O I, Cêrny R, Gladyshevskii R E and Yvon K 1995 *J. Alloys Compd.* **219** 135
[12] Bachmetew E 1934 *Z. Kristallogr.* **88** 179
[13] Popčević P *et al* 2010 *Phys. Rev.* B **81** 184203
[14] Que Z P unpublished results
[15] Kattner U R and Burton B P 1993 *Phase Diagrams of Binary Iron Alloys* ed H Okamoto (OH: ASM International, Materials Park) p 12
[16] Sundman B, Ohnuma I, Dupin N, Kattner U R and Fries S G 2009 *Acta Mater.* **57** 3896
[17] Mihalkovič M and Widom M 2012 *Phys. Rev.* B **85** 014113
[18] Li X L, Scherf A, Heilmaier M and Stein F 2016 *J. Phase Equilib. Diffus.* **37** 162
[19] Zienert T and Fabrichnaya O 2018 *J. Alloys Compd.* **743** 795
[20] Klaver T P C, Madsen G K H and Drautz R 2012 *Intermetallics* **31** 137
[21] Ledieu J, Gaudry É, Serkovic Lolo L N, Alarcon Villaseca S, de Weerd M-C, Hahne M, Gille P, Yu G, Dubois J and Fournée V 2013 *Phys. Rev. Lett.* **110** 076102
[22] Mitilainen A *et al* 2015 *Phys. Rev.* B **92** 014109
[23] de Laissardière G T, Nguyen-Manh D and Mayou D 2005 *Prog. Mater. Sci.* **50** 679
[24] Griger A, Sterfaniay V and Turmezy T 1986 *Z. Met.kd* **77** 30
[25] Fang C M, Sluiter M H F, van Huis M A and Zandbergen H W 2010 *Phys. Rev. Lett.* **105** 055503
[26] Fang C M and van Huis M A 2017 *Heliyon* **3** e00408
[27] Kresse G and Hafner J 1994 *Phys. Rev.* B **49** 14251
[28] Perdew J P, Burke K and Ernzerhof M 1996 *Phys. Rev. Lett.* **77** 3865
[29] Blöchl P E 1994 *Phys. Rev.* B **50** 17953
[30] Amador C, Lambrecht W R L and Segall B 1992 *Phys. Rev.* B **46** 1870
[31] Fang C M, van Huis M A and Sluiter M H F 2016 *Acta Mater.* **103** 273
[32] Monkhorst H J and Pack J D 1976 *Phys. Rev.* B **13** 5188
[33] Arblaster J W 2018 *Selected Values of The Crystallographic Properties of The Elements* (Ohio: ASM International, Materials Park)
[34] Zhang C-H, Huan S, Shen J and Chen N-N 2014 *Intermetallics* **52** 88
[35] Oelsen W, Middel W and Mitt W 1937 *K. W. Inst. Eisenforschung* **19** 1
[36] Biltz W 1937 *Z. Met.kd.* **29** 73
[37] Kubaschewski O and Dench W A 1955 *Acta Metall.* **3** 339
[38] Zheng W, He S, Selleby M, He Y, Li L, Lu X-G and Ågren J 2017 *Calphad* **58** 34
[39] Albedah M A, Nejadsattari F, Stadbik Z M and Przewoźnik J 2015 *J. Alloys Compd.* **619** 839
[40] van der Kraan A M and Buschow K H J 1986 *Physica* B+C **138** 55
[41] Chuang Y-Y, Schmid R and Chang Y A 1985 *Metall. Trans.* A **16** 153
[42] Fang C M, de Groot R A, Bischoff M M and van Kempen H 2000 *Surf. Sci.* **445** 123
[43] Wolverton W 2001 *Acta Mater.* **49** 3129
[44] Inden G 1981 *Physica* **103B** 82
[45] Fang C M, van Huis M A, Xu Q, Caca R J and Zandbergen H 2015 *J. Mater. Chem.* C **3** 651
[46] Chen H-L, Chen Q, Du Y, Bratberg J and Engström A 2014 *Trans. Nonfererrous Met. Soc. China* **24** 2041